Sociedade Brasileira de Automática (SBA)
XXV Congresso Brasileiro de Automática - CBA 2024, 15 a 18 de outubro de 2024

# Validation of an Isolated System for Renewable Hydrogen Production through Offshore Wind Power using OPAL-RT

**Janito Ramos**[‡] [*] **Christian Couto** [*] **Thyago Estrabis** [*] **Robson Dias** [*]

[*] *Electrical Engineering Program, Federal University of Rio de Janeiro, Rio de Janeiro, RJ, Brazil*

[‡] e-mail: janito.ramos@coppe.ufrj.br

**Abstract:** Expanding the range of available and affordable low-carbon technologies becomes increasingly important to achieve the goal of net-zero emissions by 2050 and meet the increasing global targets for sustainable energy. Offshore wind energy for renewable hydrogen production is seen as a viable option and a compelling example of a technology ready to make a significant difference in future energy systems. On the other hand, this system has some complexity in modeling and analyzing Brazilian scenarios. The literature reflects this complexity, not including a detailed technical analysis of implementing hydrogen production projects using offshore wind energy in Brazil. Then, this work validates through a Real-Time (RT) simulation an islanded microgrid system for renewable hydrogen production from an Offshore Wind Farm (OWF) of 120 MW, a 12 MW battery energy storage system (BESS), and a 120 MW electrolysis system with 6 polymer electrolyte membrane (PEM) electrolyzers, each with a capacity of 20 MW. The system control is divided into two levels: the top level, at which the Power Management System (PMS) control sets the references to the local control of each component of the system, which is represented as the bottom level control. Wind speed data is obtained using the ERA5 database, which covers a maximum distance of 50 km from the Port of Açu, located in the northern part of Rio de Janeiro State. Experimental simulations show detailed hydrogen production, the system's dynamics for different weather conditions, and stability monitoring through the Voltage- and Frequency-curve.

*Keywords:* Hydrogen; Electrolyzer; Offshore wind, Renewable energy; Real-time simulation.

## 1. INTRODUCTION

To achieve the goal of net zero emissions and meet global sustainable energy goals, it is increasingly crucial to expand the range of available and affordable low-carbon technologies (Ibrahim et al., 2022). The energetic transition is an urgent topic involving climate change, where challenges to decarbonization were defined. The Conference of the Parties (COP) defined an ambitious goal: global net human-caused carbon dioxide emissions ($CO_2$) need to reach net zero around 2050. This energetic transition scenario highlights sustainable alternatives, such as renewable hydrogen, ammonia, biofuels, synthetic fuels, and biomethane (Bouckaert et al., 2021).

One alternative to producing low-carbon technologies and fuels is using renewable energy sources such as Wind Power, Solar Power, and Wave Energy Converters. Many research studies and proposed systems focus on hydrogen production, where renewable hydrogen is primarily an energy carrier and a precursor to hydrogen-based fuels (synthetic fuels like methane, methanol, ammonia, etc.) (Ramakrishnan et al., 2024).

Many studies use offshore wind for hydrogen production, mainly for techno-economic analysis (Giampieri et al., 2024; Egeland-Eriksen et al., 2023). The offshore wind is due to the high capacity factor of generated wind power, around 60–70%, 4–5 times that of onshore locations (Ramakrishnan et al., 2024).

The production of hydrogen from renewable energy sources has shown promise in Brazil due to abundant renewable energy potential. A significant part of such potential originates from offshore renewables. According to Vinhoza and Schaeffer (2021), Brazil's offshore wind potential is 1688 GW of Gross Potential, 1064 GW of Technical Potential, and 330 GW of Environmental and Social Potential.

According to the authors' literature review, no published work addresses the detailed technical analysis of implementing hydrogen production projects using offshore wind energy in Brazil. This article proposes to cover a technical analysis gap with dynamic simulation.

This paper uses OPAL-RT Simulator to develop the real-time simulation of an islanded microgrid system for hydrogen production from an Offshore Wind Farm on the Brazilian coast. The location of the hydrogen production plant was considered in two distinct scenarios: offshore and onshore. The proposed system model is designed taking electric considerations and for the simulation, a temporal resolution of 10 minutes was considered for the wind speed data that covers a maximum distance of 50 km from the

Port of Açu, located in the northern part of Rio de Janeiro State. The results compare the monthly hydrogen production and capacity factor for two scenarios and analyze the system simulation's transient response.

The paper is organized as follows: Section 2 explains the proposed system; Section 3 presents the model and control of each component of the system; Section 4 shows the main results and discussion obtained, and Section 5 presents the main conclusion of the article.

## 2. SYSTEM DESCRIPTION

The proposed system comprises electricity generation through wind farms, an electrolysis system for hydrogen production, and a Battery Energy Storage System (BESS). Two scenarios, offshore and onshore hydrogen production, are proposed for the centralized electrolysis system model, as shown in Figures 1 and 2, respectively (Ibrahim et al., 2022).

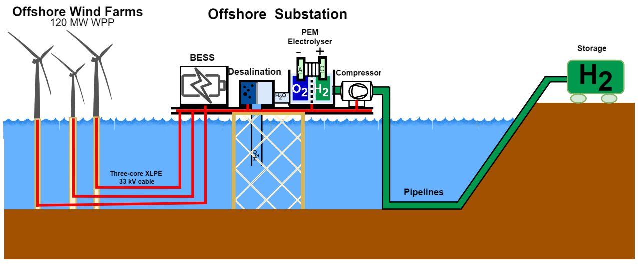


Figure 1. Offshore scenario of hydrogen production using offshore wind.

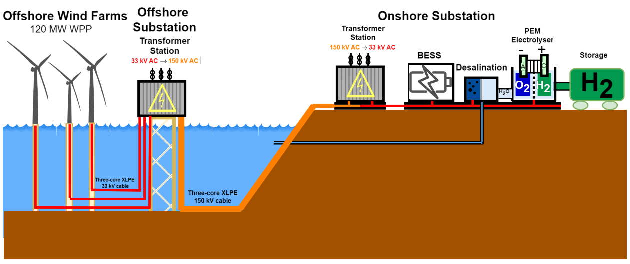


Figure 2. Onshore scenario of hydrogen production using offshore wind.

The difference between plant the two scenarios is the location of hydrogen production. In the offshore scenario, hydrogen production occurs at the offshore substation where the electrolysis facility is installed. The hydrogen produced using offshore wind power output is then transported to the shore through hydrogen pipelines. In the onshore scenario, hydrogen production takes place on the shore. The offshore substation collects the produced power and transmits it through submarine electric cables to the shore, where it is then converted to hydrogen.

The generated electricity is used for water desalination, a PEM electrolyzer, and a compressor to adjust the hydrogen pressure for storage, transportation (only in the offshore scenario), and BESS charging.

The proposed system operates independently from the grid, and the BESS is used as the grid-forming (GFM) component.

### *Generation and Transmission System*

The electricity generation system consists of a wind park with 10 wind turbines (WT) of 12 MW, each with a rotor diameter of 216.9 m and a hub height of 131.7 m, according to SINTEF (Souza et al., 2021). The 12 MW wind turbine is selected in an initial analysis of the LCOE (Levelized Cost of Energy) and LCOH (Levelised Cost of Hydrogen). The analysis is carried out considering the 10 (Bortolotti et al., 2019), 12 (Souza et al., 2021), and 15MW (Gaertner et al., 2020) wind turbines for offshore and onshore scenarios as shown in Tables 1 and 2 (Nilsson, 2023). This system uses wind turbines with transformers to increase the RMS line voltage to a typical collection voltage level of 33 kV (Ibrahim et al., 2022; Lakshmanan et al., 2021). For the onshore scenario, an offshore transformer increases the voltage from the wind farm collection point of 33 kV to 150 kV for transmission using HVAC (High Voltage Alternating Current) technologies to the shore (Pillay and Musasa, 2022). A transformer stepped down the voltage at the onshore substation for the electrolysis system connection and auxiliaries.

Table 1. Overall of the LCOE and LCOH for offshore scenario considering wind turbines of 10, 12, and 15MW

| Parameter | 10MW | 12MW | 15MW |
|---|---|---|---|
| Minimum LCOH ($/ kg) | 4.57 | 4.24 | 4.58 |
| Annual H2 Production (ton) | 10067.03 | 10720.93 | 9793.63 |
| LCOE ($/MWh) | 42.74 | 38.14 | 41.37 |

Table 2. Overall of the LCOE and LCOH for onshore scenario considering wind turbines of 10, 12, and 15MW

| Parameter | 10MW | 12MW | 15MW |
|---|---|---|---|
| Minimum LCOH ($/ kg) | 4.81 | 4.44 | 4.83 |
| Annual H2 Production (ton) | 9754.17 | 10433.71 | 9452.36 |
| LCOE ($/MWh) | 54.87 | 49.03 | 53.85 |

### *PEM Electrolysis System*

The electrolysis system of 120MW using NEL and Cummins' electrolyzers with different capacities is considered a PEM electrolyzer for hydrogen production. In this case, electrolyzers of 2.5 (NEL, 2020), 5 (Lee et al., 2022), and 20MW (Budding, 2020) are analyzed considering the LCOE and LCOH. The result is similar for hydrogen production. However, the cost of the electrolysis system with an electrolyzer of 20MW is cheaper than others, as was shown in Table 3.

Table 3. Overall of the minimum LCOH for electrolyzers of 2.5, 5, and 20MW with wind turbine SINTEF 12MW

| Electrolyzer | MC500 | HyLYZER 1000 | HyLYZER 5000 |
|---|---|---|---|
| capacity (MW) | 2.5 | 5.0 | 20.0 |
| LCOH ($/ kg) (offshore scenario) | 5.41 | 4.62 | 4.24 |
| LCOH ($/ kg) (onshore scenario) | 5.66 | 4.82 | 4.44 |

The hydrogen plant includes six Cummins HyLYZER 5000 PEM water electrolyzers (Inc., 2023) with a total capacity of 24000 $Nm^3/h$. In addition to the PEM electrolysis stacks, the hydrogen production plant includes a Balance of Plant (BoP) designed to provide the proper conditions for operating the PEM electrolyzer.

## 3. MODELING AND CONTROL OF HYDROGEN PRODUCTION PROCESS

The main components of the proposed systems are the Wind park system, which generates electricity; the PEM electrolyzer, which produces hydrogen; the auxiliaries loads (Desalination, electrolyzer's balance of plant—BoP and compressor); the BESS, which regulates the grid and stores the electricity generated; and the PMS that makes the management of the grid.

### *3.1 Wind Turbine System*

The wind turbine system could be modeled as an overall configuration of Type-4 WT, which consists of a permanent magnet synchronous generator (PMSG), a back-to-back (BTB) converter including a machine-side converter (MSC), and a grid-side converter (GSC), a DC chopper, transformer, and grid filters.

The offshore WT model is based on the equations of power ($P_{WT}$) and mechanical torque ($T_{WT}$) as a function of the wind speed. $P_{WT}$ and $T_{WT}$ are as (1) and (2), respectively.

$$P_{WT} = \frac{1}{2}\rho\pi R^2 C_p(\lambda,\beta) V_{WT}^3, \tag{1}$$

$$T_{WT} = \frac{P_{WT}}{\omega_r} = \frac{1}{2}\rho\pi R^3 C_p(\lambda,\beta) V_{WT}^2, \tag{2}$$

where $C_p$ is a power coefficient, $\rho$ is the air density ($kg/m^3$), R is the WT rotor radius ($m$), $V_{WT}$ is the wind speed ($m/s$), $\omega_r$ is the WT rotor speed ($rad/s$), $\beta$ is the pitch angle (°), and $\lambda$ is the tip-speed ratio (TSR), which is

$$\lambda = \frac{\omega_r R}{V_{WT}}. \tag{3}$$

$C_p$ is applied to represent the WTs aerodynamic characteristics, and the $C_p(\lambda,\beta)$ reflects the efficiency of wind energy conversion expressed in (4). The $C_p$ is obtained through experimental tests conducted by the manufacturer. Different equations of $Cp$ can be found in (Castillo et al., 2023). This work considers the approach in (Kotti et al., 2014) for a WT with three blades and variable speed.

$$C_p(\lambda,\beta) = 0.5(\frac{116}{\lambda_i} - 0.4\beta - 5)e^{-\frac{21}{\lambda}} + 0.0068\lambda, \tag{4}$$

$$\frac{1}{\lambda_i} = \frac{1}{\lambda + 0.08\beta} - \frac{0.035}{1+\beta^3}, \tag{5}$$

where $\lambda_i$ is an intermediate variable expressed in (5).

The main parameters of the WT and PMSG are shown in Table 4.

The main control system of wind turbines includes a pitch control, a machine-side converter control, and a grid-side converter control (Nguyen et al., 2022), as shown in Fig. 3. The pitch control regulates the blade pitch angle in high wind speed conditions or curtailing wind power.

Table 4. Electromagnetic design of the 12-MW reference direct-drive generator (Souza et al., 2021).

| Parameter | Description | Value | Units |
|---|---|---|---|
| $P_r$ | Rated Power | 12 | MW |
| $\omega_r$ | Rated speed | 0.8168 | rad/s |
| $f_e$ | Electrical frequency | 13 | Hz |
| $T_r$ | Rated Torque | 14.6 | MNm |
| $V$ | RMS line voltage | 3933 | V |
| $I$ | Nominal current(RMS) | 1077.15 | A |

The grid-side controller maintains the BTB converter's DC-link voltage, whereas the machine-side controller regulates generator torque. Both the grid-side and machine-side controllers have a cascade control structure consisting of an inner current loop and an outer DC-link voltage control or torque control loop. Proportional-integral (PI) regulators regulate voltage and current in the dq frame.

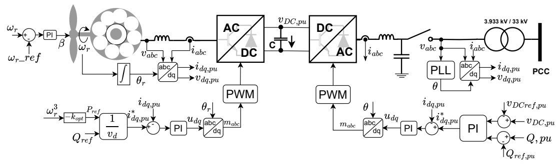


Figure 3. Schematic diagram of the control system of wind turbines.

The machine-side control strategy is a Maximum Power Point Tracker (MPPT) controller in dq-frame to ensure maximum power extraction from wind using optimal power control (OPC) (Nguyen et al., 2022). The optimal mechanical power ($P_{WT\_opt}$) produced by the turbine rotor is given by (1) (Nguyen et al., 2022). Equations (6) and (7) can be derived from (1):

$$P_{WT\_opt} = k_{opt}\omega_r^3, \tag{6}$$

$$k_{opt} = 0.5\rho\pi R^2 C_{p\_max}(\lambda,\beta)(\omega_r R/\lambda_{opt})^3. \tag{7}$$

The complete model of Fig. 3 was simplified. The lookup table $P_{WT} vs V_{WT}$ with time delay (inertia time constant of WT) is used to estimate the power of the wind park, and the controlled current source replaced the PMSG and machine-side converter control for model optimization. This change does not affect the results compared to the detailed model and improves data processing. The controlled current source is connected in parallel with a capacitor and grid-side converter in the DC link. The grid-side converter is simulated using an average Voltage-Source Converter (VSC) model. The wind turbines' transformer is connected to the AC side of the VSC, generating reactive power (Q) in the wind park. This reactive power (Q) is compensated through the reactive control to zero in the PCC (Point of Common Coupling).

### *3.2 BESS*

The hydrogen production occurs in islanded mode, and the BESS controls the frequency and voltage in grid-forming mode (Lasseter et al., 2019; Ramachandran et al., 2019). This is achieved using the droop control method (Jasim and Jasim, 2022; Arangarajan et al., 2016; Salem et al., 2023).

Using the droop control method, a grid-forming converter is a voltage source that mimics the functionality of synchronous generators. Therefore, the idea is also called virtual synchronous generators (Jasim and Jasim, 2022; Arangarajan et al., 2016; Zhao et al., 2021). In real synchronous generators, due to the inertia, when the required power increases, their frequency reduces and, in turn, decreases the power angle.

In grid-forming mode, the BESS must regulate the frequency and voltage of the Point of Common Coupling (PCC) bus. Droop control has two following functions: it controls real power (P) through frequency (F) control and controls reactive power (Q) through voltage (V) control. Regulating the system's real and reactive power allows for the manipulation of voltage and frequency. The BESS has a droop P/F of 0.5 %, meaning the frequency can fluctuate between 60.3 Hz (the inverter absorbs its nominal active power) and 59.7 Hz (the inverter produces its nominal active power). The droop Q/V is adjusted to 3%, allowing the voltage at the PCC bus to vary between 33,990.0 V (the inverter absorbs its full inductive power) and 32,010.0 V (the inverter produces its full capacitive power).

As a result, it is possible to determine the frequency and voltage droop regulation using (8) and (9), respectively.

$$f = f_{ref} - Df * P, \tag{8}$$
$$V = V_{ref} + Dv * Q, \tag{9}$$

where $f$, $V$, $P$, and $Q$ are the measured values of frequency, voltage, active power, and reactive power, respectively, from the BESS primary bus, and $f_{ref}$, $V_{ref}$, $P_{ref}$ and $Q_{ref}$ are the set values of frequency, voltage, active power, and reactive power, respectively. $Df$ and $Dv$ are the droop proportional constants.

The main control system of BESS includes a droop control, a voltage loop control, and a current loop in a cascade structure, as shown in Fig. 4.

The PI voltage regulators use the reference voltage ($V_{dref}$ and $V_{qref}$) and the measured voltage ($V_{d\_pri,pu}$ and $V_{q\_pri,pu}$) to calculate the reference currents ($i^*_{dq,pu}$). The Current Regulators use the measured and reference currents ($i_{dq,pu}$ and $i^*_{dq,pu}$) to generate the inverter's dq voltages ($udq$). Current regulators achieve a high dynamic response by utilizing feedforward computation.

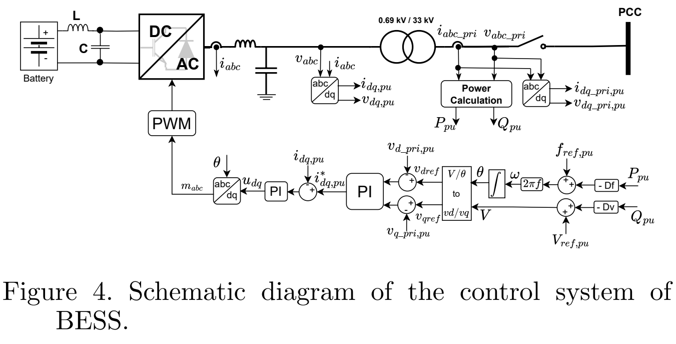


Figure 4. Schematic diagram of the control system of BESS.

The BESS is sized to support the electrolyzer when the wind farm generates less than 10 % of its nominal power for a determined time. The BESS is designed to have 10 % of the power of OWF and a nominal discharge duration of 2 hours, 12 MW/24 MWh for OWF of 120 MW.

The electrical BESS specifications are based on Saft's Intensium Shift lineup (Li-ion battery containers), shown in Table 5, considering 9 containers (3 for each 4 MW) (SAFT, 2022). This compact and modular AC BESS system enables utility-scale storage solutions for renewable energy and power grids. It is scalable up to Gigawatt-hours in size (SAFT, 2022).

Table 5. BESS specifications (SAFT, 2022).

| Parameter | Value |
|---|---|
| AC power | 4 MW |
| Nominal discharge duration | 2 hours |
| MV voltage connection | up to 36 kV |
| AC voltage | 690 V |
| DC voltage | 1500 V |
| Number of containers per lineup | 3 |
| Auxiliary consumption | 840kWh/day |
| Ambient temperature | -20°C to +45°C |
| Functions | Islanding, Grid forming, Black start, Reactive power control |

*3.3 PEM electrolyzer*

The PEM electrolyzer model developed in this article includes a mathematical model to estimate the voltage in the stack and hydrogen production, as well as a two-stage power converter design and control.

A mathematical model of the PEM electrolyzer is divided into Anode and Cathode chambers and Voltage (Liso et al., 2018; Egeland-Eriksen et al., 2023).

The electrolysis process is the reaction depicted by the breakdown of the water ($H_2O$) molecule into hydrogen ($H_2$) and oxygen ($O_2$). The external circuit with DC current provides the electromotive force for the electrochemical reaction. The basic reactions take place at the electrolyte/electrode interface. At the anode side, $H_2O$ is introduced and then split into hydrogen ions and oxygen gas. Hydrogen-positive ions cross the membrane and recombine at the cathode side, forming hydrogen gas. The basic reactions are given below the (10), (11), and (12).

$$\text{Anode: } H_2O \rightarrow 2H^+ + \frac{1}{2}O_2 + 2e^-. \tag{10}$$

$$\text{Cathode: } 2H^+ + 2e^- \rightarrow H_2. \tag{11}$$

$$\text{Net reaction: } H_2O \rightarrow H_2 + \frac{1}{2}O_2. \tag{12}$$

In the anode chamber, four moles of oxygen are produced for every electron, in accordance with Faraday's law. The molar flow rate for the oxygen produced is given by (13). Similarly, two moles of water are consumed for each electron as (14).

At the cathode side, hydrogen is calculated using Faraday's law, considering that for two moles of electrons one mole of hydrogen is generated as (15).

$$N^{gen}_{an,O_2} = \frac{I}{4F}[mol/s]. \tag{13}$$

$$N^{gen}_{an,H_2O} = \frac{I}{2F}[mol/s]. \tag{14}$$

$$N^{gen}_{cat,H_2} = \frac{I}{2F}[mol/s]. \tag{15}$$

$I$ is the current, a function of the current density, $i$, and the cell area, $A$, i.e., $I = iA$.

The electrolyzer voltage is the sum of the cell potential at open circuit ($Voc$), activation over potential ($Vact$), ohmic overpotential ($Vohm$), and concentration overpotential ($Vcon$) as (16).

$$V = V_{act} + V_{ohm} + V_{con} + V_{oc}. \tag{16}$$

The four voltage components included in this model are described in Liso et al. (2018).

The PEM electrolyzer uses a two-stage converter model (Hossain et al., 2023; Nguyen et al., 2021). The electrolyzer cell stack is connected to the DC bus through DC/DC buck converters and to the AC bus via an AC/DC rectifier and transformer, as illustrated in Fig. 5.

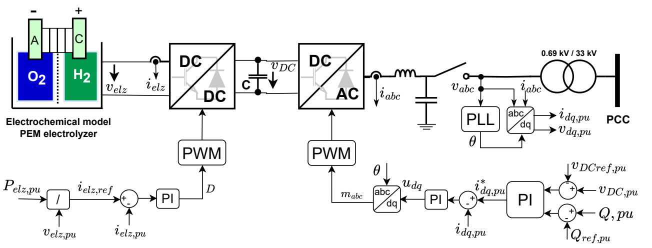


Figure 5. Schematic diagram of the control system of the electrolyzer.

The AC/DC converter controls the voltage of the DC link in the outer loop and the current in the inner loop by using PI regulators in the dq frame. On the other hand, the DC/DC buck converter is designed to regulate the current of the electrolyzer ($i_{elz}$), which functions as an electrical load.

The PEM electrolyzer nominal power was defined according to the offshore wind farm as this study includes only off-grid operation. Hence, the energy generated must be consumed at the hydrogen plant location. For this reason, the electrolysis plant capacity was chosen to match the wind farm's nominal power. These devices can operate as independent modules, which enables reaching the wind farm power by adding more electrolysis units. Moreover, they have a wide range of operations that allows them to operate under their nominal power when wind energy is scarce.

As mentioned in Table 3, three PEM electrolyzer solutions have been considered. The Cummins HyLYZER 5000 is chosen, and the relevant specifications of these PEM electrolyzer hydrogen production are included in Table 6.

As seen in Table 6, the HyLYZER 5000 has a nominal power of 20 MW. This means that to match the wind farm's nominal power, it needs 6 units.

Table 6. Hydrogen Production Specs

| **Specification** | **HyLYZER 5000** |
|---|---|
| Manufacturer | Cummins |
| Nominal Power ($MW$) | 20.0 |
| Voltage – Electrolyzer ($kV$) | 4.1 – 36 |
| Frequency ($Hz$) | 60 ± 3% |
| Hydrogen Production ($Nm^3/h$) | 4000.0 |
| Operating Pressure ($barg$) | 30.0 |
| Dynamic Range (%) | 5 to 125 |
| Ramp-up ($s$) | < 10 |

### *3.4 Power Management System*

The control system involves top- and bottom-level control, as shown in Fig. 6. In the top-level control, the Power Management System (PMS) operates the system components for the reliable operation of the system, which ensures the power equilibrium in the islanded microgrid (Bharatee et al., 2022). The PMS must guarantee a proper power allocation to the integrated devices, such as management of the PEM module according to available power and SOC (State of Charge) regulation of storage systems. The bottom-level control is a local control of each subsystem (e.g., wind park, BESS, electrolyzer, and other loads) presented in Figs. 3, 4, and 5.

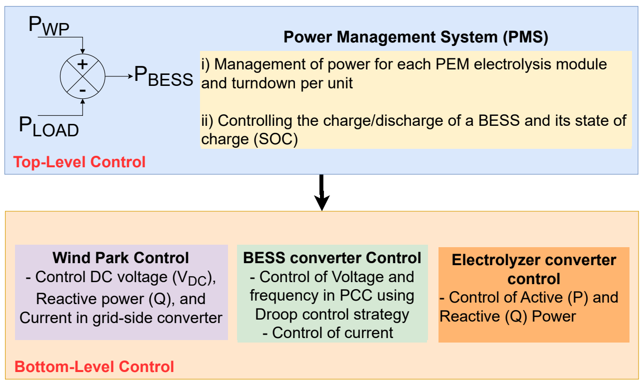


Figure 6. Control level of hydrogen production system.

The PMS is based on simple logical switches and relational operators that decide which components should receive energy from the wind turbine, as shown in Fig. 7. These decisions are made based on the magnitude of the incoming wind power and BESS SOC.

The SOC range of the BESS is set to be 20 – 80 %, i.e., charging is switched off when the SOC reaches 80 %, and discharging is switched off when the SOC gets down to 20 %. As a grid-forming component of the microgrid, the PMS prioritizes charging the BESS when its SOC is lower than 30 %.

The electrolysis system operates when the wind power is greater than 10 % of the combined rated power of the electrolyzer and hydrogen compressor (minimum electrolyzers power). If the wind power output is lower than 10 %, then the battery is used to supplement the wind power and ensure that the minimum required power is maintained to keep the electrolyzers running. This is done if the BESS SOC is greater than 30%. However, if the SOC is lower than 30 %, the electrolyzer is switched off to avoid excessive on/off-switching of the electrolyzers when

ISSN: 2525-8311

DOI: 10.20906/CBA2024/4527

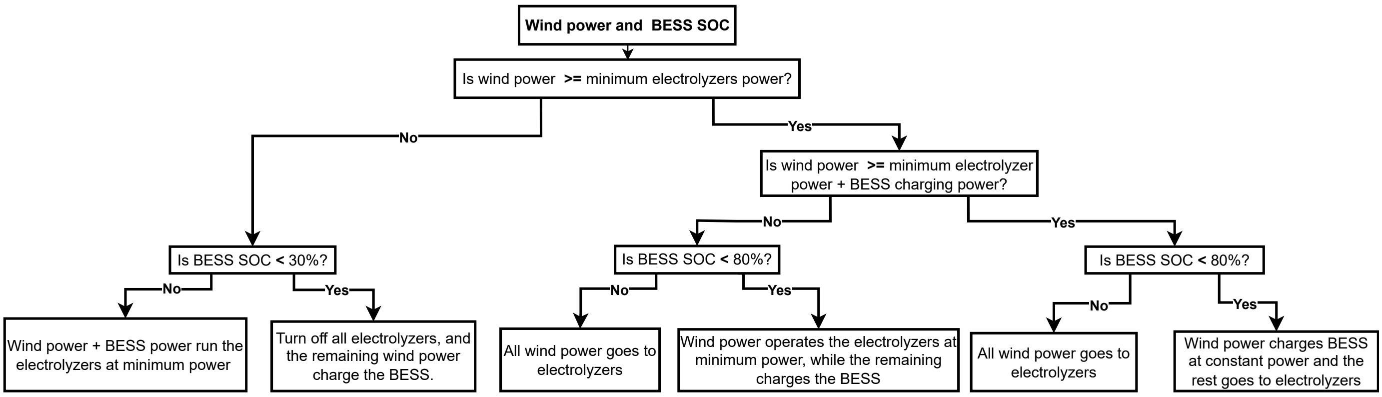


Figure 7. Overview of Power Management System algorithm.

the wind turbine fluctuates in the low power range and the wind power charges the BESS.

When the wind power is greater than or equal to the combined 10 % of the power used for electrolysis and the nominal charging power, the system prioritizes charging the BESS until its SOC reaches 80%. Once the BESS SOC reaches 80%, all wind power is directed towards the electrolysis system.

When the wind power is greater than the minimum electrolyzers power but lower than the combined minimum electrolysis power and BESS nominal charging power, the system prioritizes keeping the electrolysis system on while using the remaining wind power to charge the BESS. However, if the SOC reaches 80 %, all wind power will go to the electrolysis system.

## 4. RESULTS AND DISCUSSION

The Hydrogen Production System was simulated and validated using Software-in-the-Loop (SIL) with real-time Simulator OPAL-RT 5700, as shown in Figure 8.

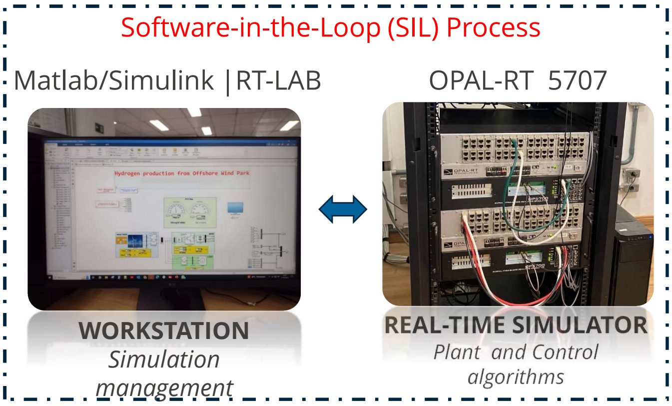


Figure 8. Simulation setup in OPAL-RT.

The offshore and onshore system simulations use the waked velocity of each wind turbine, considering the wake effects, for optimized wind park layout. The data includes a time series of average wind speeds every ten minutes for one year. Based on wind speed, the ideal power output of the wind park can be estimated using the power curve shown in Figure 9. The results show the highly variable nature of wind power, which poses a significant challenge to the control system, particularly in island mode. The power curves indicate a high capacity factor of around 80% for a wind park in December, while the low capacity factor is around 29%.

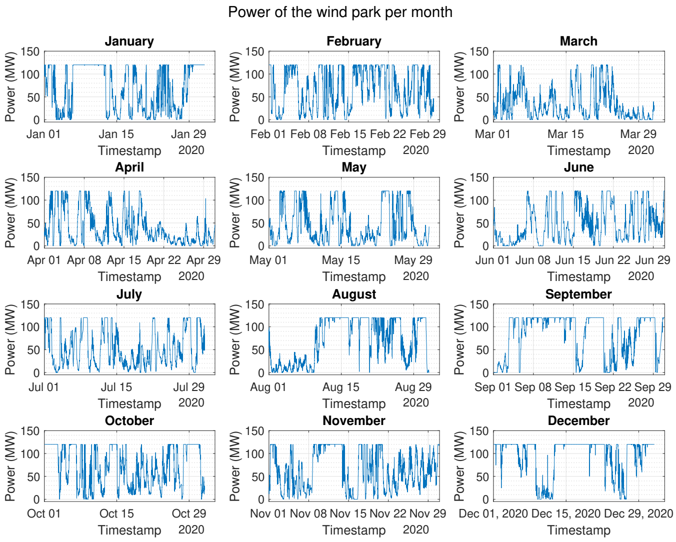


Figure 9. Power curves for each month.

For system validation, the simulation was run for offshore and onshore scenarios. The results, in Table 7, present the monthly hydrogen production (in tons) and the capacity factor of the electrolyzer.

Table 7. Results of hydrogen production and capacity factor for the offshore and onshore scenario.

| Mouth | Hydrogen production (tons) | | Capacity Factor | |
|---|---|---|---|---|
| | Offshore | Onshore | Offshore | Onshore |
| January | 987.1 | 971.7 | 0.68 | 0.67 |
| February | 896.7 | 877.5 | 0.62 | 0.61 |
| March | 473.4 | 459.0 | 0.33 | 0.32 |
| April | 519.0 | 506.3 | 0.36 | 0.35 |
| May | 636.2 | 623.1 | 0.44 | 0.43 |
| June | 652.2 | 641.4 | 0.45 | 0.44 |
| July | 747.5 | 725.5 | 0.52 | 0.50 |
| August | 1004.9 | 990.4 | 0.69 | 0.68 |
| September | 1148.9 | 1128.4 | 0.79 | 0.78 |
| October | 989.3 | 965.8 | 0.68 | 0.67 |
| November | 881.6 | 859.9 | 0.61 | 0.59 |
| December | 1362.8 | 1338.3 | 0.94 | 0.92 |

According to Table 7, the offshore scenario has a hydrogen production and capacity factor greater than the onshore scenario. In an onshore scenario, there is an added loss in the transmission cable. December had the highest hydrogen production and capacity factor at 1362.8 tons and 94 %, respectively, while March had the lowest at 459 tons and 32 %. The offshore and onshore scenarios produced a total of 10299.7 and 10087.2 tons of hydrogen, respectively, at a capacity factor of 59 % and 58 %.

Figures 10 and 11 display Active Powers, PCC voltage and frequency, the voltage of each electrolyzer, instantaneous hydrogen production, and the voltage, current, and SOC of BESS over 48 hours in April and December, respectively. The curves show how the system control changes for different system conditions.

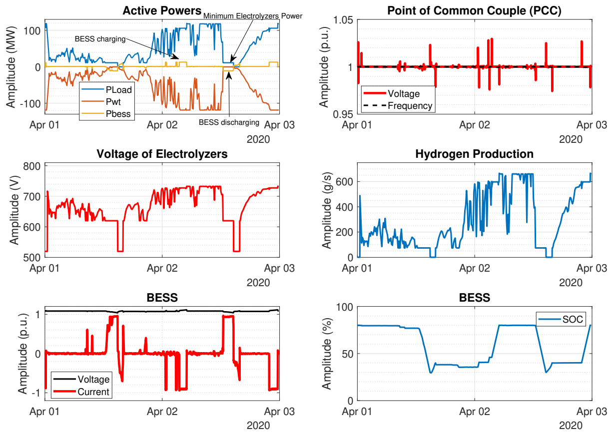


Figure 10. Simulation results for 1st and 2nd April.

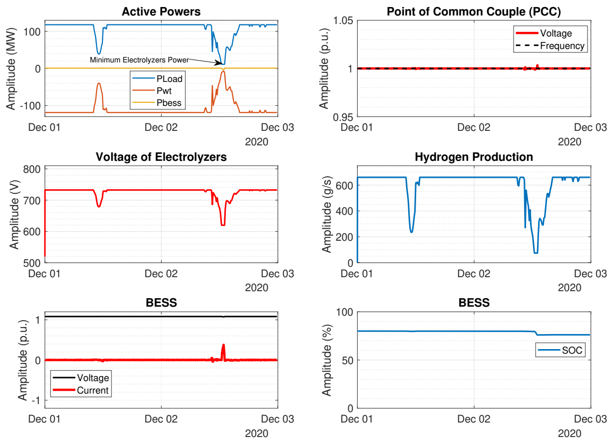


Figure 11. Simulation results for 1st and 2nd December.

According to Figures 10 and 11, the active power of the BESS (Pbess) is determined by the balance between the active wind power (Pwt), the active load power (Pload), and the SOC of the BESS. Initially, the SOC is around 80 %, and the wind power is used to supply the load, including electrolyzers and auxiliaries. If the wind power is insufficient to power the electrolyzers, the BESS power is used to supplement the generation power and keep the electrolyzers running, resulting in BESS discharging, as indicated in Figure 10. Once the BESS SOC drops below 30%, the electrolyzers are shut down (if the wind power is insufficient), and the BESS begins charging. When wind power is high, the BESS is charged to maintain its SOC near 80%. So, the BESS SOC was maintained between 30% and 80 %.

The BESS as GFM ensured the PCC voltage and frequency were within the range established by Droop control. Figure 10 shows that despite the high variability in power, the voltage and current remain near 1 p.u.

Electrolyzers voltage and hydrogen production vary in value according to the available power. The voltage of the electrolyzers varies between 520 and approximately 735 V, while hydrogen production varies between 74 and 660 g/s.

## 5. CONCLUSION

This paper presented the real-time simulation of an islanded microgrid system for renewable hydrogen production from an Offshore Wind Farm using OPAL-RT. BESS operates in GFM mode using droop control. The article considers the location of hydrogen production in two distinct scenarios: offshore and onshore, with the wind speed data obtained from the Port of Açu, located in the northern part of Rio de Janeiro State.

The monthly hydrogen production results and the electrolyzers' capacity factor for wind speed data during a year with a temporal resolution of 10 minutes are presented. The main curves of the system simulation are shown, such as powers curves, voltage and frequency of PCC, the voltage of electrolyzers, instantaneous hydrogen production, and BESS curves.

The results show that the offshore scenario has a greater hydrogen production and capacity factor than the onshore scenario. The simulation's dynamic response shows good performance of the PMS algorithm, which supplies the reference for each system component. The local control of each component performs better and maintains stability for different system conditions.

In the future, it is suggested that a simulation of the hydrogen production system, specifically in grid-connected mode, be created. The simulation should incorporate solar photovoltaic systems as renewable energy sources. Additionally, the nominal power of the generation source can be increased, and the impact of renewable sources and electrolyzers connected to the grid can be analyzed. The BESS can provide support to the grid. It pretends to develop the controller Hardware-in-the-loop (CHIL) using OPAL-RT and OP8666 (DSP Controller Board for F28379D controlCARD).

## ACKNOWLEDGEMENTS

The authors thank the support of the Coordenação de Aperfeiçoamento de Pessoal de Nível Superior – Brasil (CAPES) – Finance Code 001 and TotalEnergies EP Brasil in accord to ANP Resolution 918/2023.

## REFERENCES

Arangarajan, V., KSV, S., Khoo, Y.S., Oo, A., and Stojcevski, A. (2016). Pv based microgrid with grid-support grid-forming inverter control-(simulation and analysis). *Smart Grid and Renewable Energy-Scientific Research Publishing*, 8, 1–30. doi:10.4236/sgre.2017.81001.

Bharatee, A., Ray, P.K., Subudhi, B., and Ghosh, A. (2022). Power management strategies in a hybrid energy storage system integrated ac/dc microgrid: a review. *Energies*, 15(19), 7176.

Bortolotti, P., Dykes, K., Merz, K., and Zahle, F. (2019). Iea wind task 37 on systems engineering in wind energy. *WP2-Reference Wind Turbines.: IEA Wind Task*, 37.

Bouckaert, S., Pales, A.F., McGlade, C., Remme, U., Wanner, B., Varro, L., D'Ambrosio, D., and Spencer, T. (2021). *Net zero by 2050: A roadmap for the global energy sector*. IEA. URL `https://iea.blob.core.windows.net/assets/deebef5d-0c34-4539-9d0c-10b13d840027/NetZeroby2050-ARoadmapfortheGlobalEnergySector_CORR.pdf`.

Budding, D. (2020). *Techno-economic study of a power-to-hydrogen system in offshore wind energy*. Master's thesis, University of Twente.

Castillo, O.C., Andrade, V.R., Rivas, J.J.R., and González, R.O. (2023). Comparison of power coefficients in wind turbines considering the tip speed ratio and blade pitch angle. *Energies*, 16(6), 2774.

Egeland-Eriksen, T., Jensen, J.F., Ulleberg, Ø., and Sartori, S. (2023). Simulating offshore hydrogen production via pem electrolysis using real power production data from a 2.3 mw floating offshore wind turbine. *international journal of hydrogen energy*, 48(74), 28712–28732.

Gaertner, E., Rinker, J., Sethuraman, L., Zahle, F., Anderson, B., Barter, G.E., Abbas, N.J., Meng, F., Bortolotti, P., Skrzypinski, W., et al. (2020). Iea wind tcp task 37: definition of the iea 15-megawatt offshore reference wind turbine. Technical report, National Renewable Energy Lab.(NREL), Golden, CO (United States).

Giampieri, A., Ling-Chin, J., and Roskilly, A.P. (2024). Techno-economic assessment of offshore wind-to-hydrogen scenarios: A uk case study. *international journal of hydrogen energy*, 52, 589–617.

Hossain, M.A., Islam, M.R., Hossain, M.A., and Hossain, M. (2023). Control strategy review for hydrogen-renewable energy power system. *Journal of Energy Storage*, 72, 108170.

Ibrahim, O.S., Singlitico, A., Proskovics, R., McDonagh, S., Desmond, C., and Murphy, J.D. (2022). Dedicated large-scale floating offshore wind to hydrogen: Assessing design variables in proposed typologies. *Renewable and Sustainable Energy Reviews*, 160, 112310.

Inc., C. (2023). Hylyzer®-5000 pem electrolyzer plant proposal - budgetary quotation for a 100mw electrolyzer.

Jasim, A.M. and Jasim, B.H. (2022). Grid-forming and grid-following based microgrid inverters control. *Iraqi Journal for Electrical & Electronic Engineering*, 18(1).

Kotti, R., Janakiraman, S., and Shireen, W. (2014). Adaptive sensorless maximum power point tracking control for pmsg wind energy conversion systems. In *2014 IEEE 15th Workshop on Control and Modeling for Power Electronics (COMPEL)*, 1–8. IEEE.

Lakshmanan, P., Sun, R., and Liang, J. (2021). Electrical collection systems for offshore wind farms: A review. *CSEE Journal of Power and Energy Systems*, 7(5), 1078–1092.

Lasseter, R.H., Chen, Z., and Pattabiraman, D. (2019). Grid-forming inverters: A critical asset for the power grid. *IEEE Journal of Emerging and Selected Topics in Power Electronics*, 8(2), 925–935.

Lee, S.A., Kim, J., Kwon, K.C., Park, S.H., and Jang, H.W. (2022). Anion exchange membrane water electrolysis for sustainable large-scale hydrogen production. *Carbon Neutralization*, 1(1), 26–48.

Liso, V., Savoia, G., Araya, S.S., Cinti, G., and Kær, S.K. (2018). Modelling and experimental analysis of a polymer electrolyte membrane water electrolysis cell at different operating temperatures. *Energies*, 11(12), 3273.

NEL (2020). M series mc500 system efficiency. Technical report, NEL.

Nguyen, B.L., Panwar, M., Hovsapian, R., Nagasawa, K., and Vu, T.V. (2021). Power converter topologies for electrolyzer applications to enable electric grid services. In *IECON 2021–47th Annual Conference of the IEEE Industrial Electronics Society*, 1–6. IEEE.

Nguyen, T.T., Vu, T., Paudyal, S., Blaabjerg, F., and Vu, T.L. (2022). Grid-forming inverter-based wind turbine generators: Comprehensive review, comparative analysis, and recommendations. *arXiv preprint arXiv:2203.02105*.

Nilsson, M. (2023). Offshore wind power co-operated green hydrogen and sea-water oxygenation plant: A feasibility case study for sweden.

Pillay, C.J. and Musasa, K. (2022). Comparison of hvac and hvdc collection grids in offshore windfarms. In *2022 IEEE PES/IAS PowerAfrica*, 1–5. IEEE.

Ramachandran, R., Poullain, S., Benchaib, A., Bacha, S., and François, B. (2019). On the black start of offshore wind power plants with diode rectifier based hvdc transmission. In *2019 21st European Conference on Power Electronics and Applications (EPE'19 ECCE Europe)*, P–1. IEEE.

Ramakrishnan, S., Delpisheh, M., Convery, C., Niblett, D., Vinothkannan, M., and Mamlouk, M. (2024). Offshore green hydrogen production from wind energy: Critical review and perspective. *Renewable and Sustainable Energy Reviews*, 195, 114320.

SAFT (2022). Intensium shift energy storage lineup brochure. Technical report, Intensium Shift Energy Storage lineup Brochure.

Salem, Q., Aljarrah, R., Karimi, M., and Al-Quraan, A. (2023). Grid-forming inverter control for power sharing in microgrids based on p/f and q/v droop characteristics. *Sustainability*, 15(15), 11712.

Souza, C., Berthelsen, P., Eliassen, L., Bachynski, E., Engebretsen, E., and Haslum, H. (2021). Definition of the ino windmoor 12 mw base case floating wind turbine. Technical report, Tech. Rep. OC2020 A-044, SINTEF Ocean.

Vinhoza, A. and Schaeffer, R. (2021). Brazil's offshore wind energy potential assessment based on a spatial multi-criteria decision analysis. *Renewable and Sustainable Energy Reviews*, 146, 111185.

Zhao, F., Wang, X., Zhou, Z., Harnefors, L., Svensson, J.R., Kocewiak, Ł.H., and Gryning, M.P.S. (2021). Control interaction modeling and analysis of grid-forming battery energy storage system for offshore wind power plant. *IEEE Transactions on Power Systems*, 37(1), 497–507.